Published in final edited form as:
Clin Cancer Res. 2012 October 15; 18(20): 5741–5751. doi:10.1158/1078-0432.CCR-12-1188.

Intraoperative Near-Infrared Imaging of Surgical Wounds after Tumor Resections Can Detect Residual Disease

Brian Madajewski[1], **Brendan F. Judy**[1], **Anas Mouchli**[1], **Veena Kapoor**[1], **David Holt**[2], **May D. Wang**[3], **Shuming Nie**[4], and **Sunil Singhal**[1]

[1]Department of Surgery, University of Pennsylvania School of Medicine, Philadelphia, Pennsylvania

[2]Department of Clinical Studies, University of Pennsylvania School of Veterinary Medicine, Philadelphia, Pennsylvania

[3]Department of Biomedical Engineering, Georgia Institute of Technology, Atlanta, Georgia

[4]Departments of Biomedical Engineering and Chemistry, Emory University, Atlanta, Georgia

Abstract

Background—Surgical resection remains the most effective therapy for solid tumors worldwide. The most important prognostic indicator for cure following cancer surgery is a complete resection with no residual disease. However, intraoperative detection of retained cancer cells after surgery is challenging, and residual disease continues to be the most common cause of local failure. We hypothesized visual enhancement of tumors using near-infrared imaging could potentially identify tumor deposits in the wound after resection.

Methods—A small animal model of surgery and retained disease was developed. Residual tumor deposits in the wound were targeted using an FDA approved imaging agent, indocyanine green, by the enhanced permeability and retention (EPR) effect. A novel hand-held spectrometer was used to optically visualize retained disease after surgery.

Results—We found residual disease using near-infrared imaging during surgery that was not visible to the naked eye or microCT. Furthermore, examination of tumor nodules was remarkably precise in delineating margins from normal surrounding tissues. This approach was most successful for tumors with increased neovasculature.

Conclusions—The results suggest that near-infrared examination of the surgical wound after curative resection can potentially enable the surgeon to locate residual disease. The data in this study is the basis of an ongoing Phase I/II clinical trial in patients who undergo resection for lung and breast cancer.

Keywords

intraoperative imaging; surgical oncology; infrared; margins; indocyanine green

Corresponding Author: Sunil Singhal, M.D., Assistant Professor, University of Pennsylvania School of Medicine, 6 White Building, 3400 Spruce Street, Philadelphia, PA 19104. sunil.singhal@uphs.upenn.edu.

Disclosures: One of the authors (SN) is a consultant of SpectroPath, Inc., a startup company in Atlanta,GA to develop advanced instrumentation and nanoparticle contrast agents for image-guided surgery.

Introduction

Cancer remains a major health problem and affects over 1.4 million Americans each year (1). Surgical resection is the most effective therapy for early stage solid tumors, and over 50% of patients with cancer undergo surgery with curative intent each year (2). A complete resection at the time of surgery is the single most important factor in predicting long term survival and improves the cure rate by 4 to 11 fold for many cancers (2). Unfortunately, up to 40% of patients leave the operating room with deposits of cancer cells left behind at the time of surgery (2).

Patients with recurrent disease tend to have poor outcomes (2). Local recurrences occur from cancer cells found at the edge of the resection field, or the “surgical margin”. Local recurrences are a known risk of surgery, thus radiation therapy is often given postoperatively to prevent relapses. For example, in breast cancer, after the standard-of-care lumpectomy to remove a breast nodule, adjuvant radiation is usually administered to the surgical field (3). However, radiation has significant side effects and morbidity such as scarring, collateral tissue damage and patient fatigue.

Surgeons have a limited ability to locate residual tumor cells at the surgical margin. For the last two centuries, surgeons have used their hands and their eyes to locate and evaluate these margins, but this approach has limitations. Frozen sections are typically performed during surgery to examine margins, and representative samples of the tumor margin are sent to the pathologist for rapid examination to determine if tumor cells are present. However, studies have shown that it would take 3000, 6 μm thick sections to fully evaluate the margins of a 2 centimeter breast biopsy, an impossible task intra-operatively (4, 5).

Our group and others (6–8) have been investigating the use of real-time imaging during surgery to examine tumor margins and residual neoplasia. Near infrared (NIR) imaging is a safe, low-energy (10^{-1} eV) approach to imaging and delivers 10^5 less energy than a routine chest radiograph (10^4 eV) making it safe for the surgeon, patient, and surgical team. Indocyanine green (ICG) is an innocuous, FDA-approved imaging dye that can be injected into patients and be detected by NIR imaging. ICG imaging is not possible for most diagnostic applications due to the lack of tissue penetration of the emitted light through the skin (9), however, when the body cavity is open, NIR imaging devices can detect ICG at depths of 5–10 mm in tissue.

ICG is avidly taken up in solid tumors that have “leaky capillaries” due to the enhanced permeability and retention (EPR) effect (10). The EPR effect is a property by which small molecules (ie. nanoparticles) accumulate in tumors due to the presence of defective endothelial cells and wide fenestrations that characterize neovasculature in cancer tissues (11). Although ICG is not tumor specific, for purposes of intraoperative diagnostic imaging, the identification of any abnormal tissues is more important than specificity for cancer deposits.

We hypothesized that NIR imaging could be used to detect tumor margins and discover residual tumor deposits during surgery. Since ICG is preferentially retained in tumors, we used a novel local recurrence model in small animals to test our NIR imaging platform. We found that residual tumor deposits could be detected with remarkable accuracy. There was no associated toxicity and surgical outcomes were remarkably improved by combining NIR imaging with standard of care surgical resection. This data is the basis of an ongoing clinical trial in lung cancer and breast cancer.

Materials and Methods

Mouse Studies

Female C57BL/6 (B6, Thy1.2), BALB/c, athymic Ncr-nu/nu and B6–129/J1 hybrid mice mice were purchased from Charles River Laboratories and Jackson Laboratories. All mice were maintained in pathogen-free conditions and used for experiments at ages 8 week or older. The Animal Care and Use Committees of the Children's Hospital of Philadelphia, The Wistar Institute and the University of Pennsylvania approved all protocols in compliance with the Guide for the Care and Use of Laboratory Animals.

Cell lines

The murine malignant mesothelioma cell line, AB12, was derived from an asbestos-induced tumor and has been previously described in detail (12). The murine esophageal carcinoma cell line, AKR, was derived from mouse esophageal squamous epithelia with cyclin D1 over expression via Epstein-Barr virus ED-L2 promoter in p53 deficient genetic backgrounds (13). The murine lung cancer cell line, TC1, was derived from mouse lung epithelial cells immortalized with HPV-16 E6 and E7 and transformed with the c-Ha-ras oncogene (14). The spontaneously metastatic murine lung cancer line, LKR, was derived from an explanted pulmonary tumor from an activated KrasG12D mutant mouse that had been induced in an F1 hybrid of 129Sv.J and C57BL/6 (14). The metastatic NSCLC cell line, murine Lewis lung carcinoma (LLC), was obtained from American Type Culture Collection (Manassas, VA). AE17 is an asbestos-derived murine mesothelioma cell line (kindly provided by Steven Albelda, University of Pennsylvania).

AB12, LKR, AKR, and LLC cell lines were cultured and maintained in high-glucose DMEM (Dulbecco's Modified Eagle's Medium, Mediatech, Washington DC) supplemented with 10% fetal bovine serum (FBS; Georgia Biotechnology, Atlanta, GA), 1% penicillin/streptomycin, and 1% glutamine. TC1 and AE17 cell lines were cultured in RPMI (RPMI 1640 Medium, Mediatech, Washington DC) 10% FBS, 1% penicillin/streptomycin, and 1% glutamine. Cell lines were regularly tested and maintained negative for *Mycoplasma spp.*

Green fluorescent protein (GFP) transduction of murine cancer cells *in vitro*

AE17 tumor cells were infected with the lentiviral vector pELNS bearing the EF1α promoter in order to develop GFP fluorescence. The packing of the plasmid into the lentivirus has been previously described (15). Labeled cells were confirmed to express GFP by flow cytometry and fluorescent microscopy.

Reagents

Pharmaceutical grade indocyanine green (ICG) was purchased from Akorn, Inc. (IC-GREEN™, NDC 17478-701-02, Lake Forest, IL). Animals were dosed with 7.5 mg/kg of ICG via intravenous injection 24 hours prior to imaging.

Animal flank tumor models

Mice were injected subcutaneously on the flank with 5×10^5 AKR tumor cells (C57Bl/6 mice), 1×10^6 AB12 cells (BALB/c mice), 1.5×10^6 TC1 cells (C57Bl/6 mice), 2×10^6 LLC cells (C57Bl/6 mice), or 2×10^6 LKR cells (Bl/6×129/J1) unless otherwise noted. Tumor cells for subcutaneous injections were suspended in 100μL PBS. Tumor volume was calculated using the formula $(3.14 \times \text{long-axis} \times \text{short-axis}^2)/6$.

Surgery was performed on mice bearing flank tumors using an established partial resection model (16). Surgery was performed when tumors reached ~ 800 mm^3. Mice were

anesthetized with intramuscular ketamine (80 mg/kg) and xylazine (10 mg/kg), shaved, and the surgical field sterilized prior to surgery. A 1 to 2 cm incision was made adjacent to the tumor and 80% of the tumor was removed using standard blunt dissection technique. After imaging, the incision was closed using sterile silk 4-0 sutures. Buprenorphine (0.2 mg/kg) was administered at the time of surgery and 6 hours postoperatively to provide analgesia. Preoperative treatment was unknown to the investigator performing surgery and making tumor measurements.

Canine tumor model

Three canines with spontaneously occurring soft tissue sarcomas were recruited from the University of Pennsylvania School of Veterinary Medicine. All protocols were approved by the Animal Care and Use Committees of the University of Pennsylvania and were in compliance with the Guide for the Care and Use of Laboratory Animals. Animals underwent ICG injection and soft tissue sarcomas in canines were resected by standard surgical practice. All tumors and surrounding tissues were imaged *in vivo* and *ex vivo*.

Near infrared and fluorescent imaging

The Li-Cor Pearl® Impulse (LI-COR Biosciences, Lincoln, NE) was utilized to visualize ICG present within the tissues of the animal. The IVIS® Lumina II (Caliper Life Sciences, Hopkinton, MA) was implemented to visualize GFP fluorescence expressed by the AE17-GFP cell line. Both machines are housed at the University of Pennsylvania's Small Animal Imaging Facility (Philadelphia, PA).

The hand-held near infrared imaging system has been previously described in detail (17). In brief, A Raman Probe detector was incorporated into a cylindrical stainless steel sampling head integrated with a 5 m, two-fiber cable; one for laser excitation and the other for light collection. The sampling head and fiber cable were coupled via an FC connector to a spectrometer. The combined sampling head and spectrometer system has a wavelength range of 800–930 nm with 0.6 nm spectral resolution for near infrared (NIR) fluorescence measurement. The excitation light was provided by a 785 nm, 100 mW continuous-wave diode laser.

Micro Computed axial tomography (microCT) scanning

In order to demonstrate the size of residual disease that remains after surgery, micro computed axial tomography (microCT) was performed before surgery and following surgery and wound closure. (MicroCAT II®, ImTek, Inc. Knoxville, TN) A series of 10 representative animals underwent partial or total resection of their flank tumors, and then imaged utilizing the MicroCAT II® (18).

Immunohistochemical stains

Animals were euthanized at designated intervals. Their tumors were harvested and bisected with one half either placed in Tissue-Tek OCT and stored at −80°C or in formalin for paraffin sectioning. To detect endothelial cells, monoclonal CD31 (mAB390) (19) was raised from hybridoma supernatant and purified. Frozen tumor sections were prepared as previously described (20). CD31 expression was quantified by counting the number of positively staining cells in four high-powered (×400) fields (21). Five slides for each specimen were analyzed as previously described.

Statistical analyses

For flow cytometry, immunohistochemistry, flank tumor volume studies comparing differences between two groups, we used unpaired Student's T tests. For studies comparing

more than two groups, ANOVA with appropriate post hoc testing was implemented. Kaplan-Meier curves were utilized to determine postoperative median survival. Postoperative survivals (defined as the time from surgery to the time which flank tumor volume reached 1,500 mm^3) for treatment groups were compared using the log-rank statistic. Differences were considered significant when $p < 0.05$. Data are presented as mean (standard error), unless otherwise noted.

Results

A surgical model for residual tumor after surgery develops local relapses

In order to model the human scenario for local recurrences after surgery, several flank xenografts were established in C57bl/6 and BALB/c mice. We tested non-small cell lung cancer (TC1, LLC, LKR), mesothelioma (AB12), breast cancer (4T1), esophageal (AKR) and melanoma (B16) cell lines to confirm the broad generalizability of this model. Over 7 experiments, syngeneic immunocompetent mice (n=150) were injected with tumor cells into the right flanks. In three weeks, animals developed well-encapsulated flank tumors that could be visualized and palpated (Figure 1a). Once the tumors reached a mean volume of 800 mm^3, animals underwent surgery with positive margins (n=120) or complete resection (n=30). Two independent observers were then asked to distinguish which animals had complete resection versus residual disease. They were instructed to locate any tumor deposits while the wound was open. They did not have prior knowledge about which animals underwent partial versus complete resection. The observers independently examined the wound after all bleeding had ceased but without any enhanced visual tools such as surgical loupes (Figure 1a). The observers recorded which animals had suspicious areas. After recording their decisions following visual inspection, they were then allowed to palpate the wound.

If at least one of the two observers felt there was a residual nodule, the animal was labeled as an incomplete resection. Manual palpation added little to the study. None of the residual tumors were able to be palpated by either the observer or the surgeon. The underlying pelvis or rib cage often made it difficult to distinguish bony protuberances from the actual disease. The observers were able to detect only 11 of the 120 residual tumors and falsely assigned 2 of the 30 animals with complete resection with residual tumors. Visual inspection of the wound for residual disease thus had a sensitivity of 9.2%, specificity of 93.3%, a positive predictive value of 84.6% and a negative predictive value of 20.4%. Palpation was not useful for technical reasons in small animals. MicroCT scanning has been shown to be more accurate than visual examination of flank murine tumors (18). Thus, we performed radiographic imaging of the surgical wound to determine if there are residual nodules. MicroCT scanning showed that these nodules are radiographically indistinguishable from the surrounding tissue (Figure 1a).

Animals were allowed to recover and then monitored for recurrence. Greater than 97% of all animals with partial resection developed local recurrences that could be visualized within 1 week (Figure 1b). Local recurrences rapidly developed potentially due to several factors that have been previously described, such as pre-established tumor microenvironment, perioperative immunosuppression and the presence of wound related growth factors (14, 16). Within 30 days, the local recurrences reached a large size (>800 mm^3) and the animals were euthanized (Figure 1b).

Residual tumor in the surgical bed fluoresces after incomplete resection

In order to determine if the NIR imaging platform could detect residual tumor deposits after surgery, animals with large established tumors were resected and the surgical bed was

examined for retained disease by (i) visual inspection; (ii) Li-Cor Pearl® Impulse; and (iii) the portable hand held NIR device. Syngeneic mice (n=60) were injected with TC1 tumor cells in the right flank. When tumors reached 800mm^3, animals were administered ICG, and the operating surgeon resected >95% of the tumor 24 hours later. Two independent observers were then asked to visually examine the surgical bed for residual disease (Figure 2a). If the residual disease was seen without imaging, the animal was eliminated from the study. All remaining animals (n=54) thought to be disease free were then imaged using the NIR device (Figure 2a). The entire wound bed was systemically scanned and imaged for residual disease at the margins.

Near-infrared fluorescence was recorded in 25 different locations. The mean value was designated the background fluorescence (mean fluorescence 2429 +/− 528 arbitrary units) (Figure 2b). If an area of high uptake was discovered, the tissues surrounding the suspicious region were imaged at 2 mm intervals from the focus in four perpendicular directions. NIR imaging revealed 46 animals (85%) had residual nodules. The NIR fluorescence was significantly higher in these residual nodules (mean fluorescence 41226 +/− 1429 au) compared to the average of the surrounding background fat, skin, muscle and fascial tissues. The fold difference of the center of the residual nodule was based on the background value. On average, tumors were 16.9 fold more fluorescent than the surrounding tissue (Figure 2b). Within 4 mm from the closest margin, there was residual fluorescence that was 3–5 fold higher than the background. The small size of the residual nodule did not technically permit accurate correlation of residual tumor size and fluorescent signal intensity.

In vivo, imaging on the Li-Cor Pearl® Impulse was not as sensitive as the hand held device in detecting NIR fluorescence. In 56% (n=30) of the cases, the Li-Cor Pearl® Impulse did not detect any residual disease despite high measurements of fluorescence from the NIR hand held device. The hand held NIR device did not detect residual nodules in 8 animals (15%). Eight animals were not deemed to have residual nodules by visual inspection, Li-Cor Pearl® Impulse or hand held NIR imaging. The hand held NIR device thus had a sensitivity of 85.2% (95% CI 0.72–0.93) whereas the Li-Cor Pearl® Impulse had a sensitivity of 29.6% (95% CI 0.18–0.44) in discovering residual nodules after surgery.

In order to confirm that the ICG was specific to tumor cells and not inflammatory tissues that may exist in a surgical wound, we repeated our experiments in a mesothelioma cell line (AE17) labeled with green fluorescent protein (GFP). GFP is expressed ubiquitously by the transformed tumor cells, thus we hypothesized it would be a precise method to compare the margins of tumors with near infrared fluorescence. We injected 20 immunodeficient mice with AE17-GFP tumor cells in the flank. Once the tumors reached 800mm^3, they were resected with positive margins. We imaged mice looking before and after surgery using ICG and GFP (Figure 2c). There was an exact overlay of fluorescent signals when imaged at 820 nm (ICG) and 510 nm (GFP). This confirmed that the tumor tissue was preferentially retaining ICG as compared to the surrounding normal tissue. This characteristic was not altered after surgical resection.

Residual tumor deposits have elevated fluorescent signals *ex vivo*

In order to confirm the presence of residual disease, the nodules were harvested and analyzed *ex vivo*. The residual nodules were re-imaged using the Li-Cor Pearl® Impulse and the hand held NIR machine following resection (Figure 3a). In several cases, peritumoral tissue such as fat and underlying fascia and muscle was harvested along with removal of the residual nodule. The margins of the nodule could be more easily delineated *ex vivo* using the hand held device. The lack of background noise from the mouse abdominal cavity and the ability to position the nodule flat on a dry surface improved the fluorescence readings (Figure 3a). In all cases, an additional piece of tissue distant from the tumor such as muscle,

fat and epidermis was harvested. The fluorescence signal in the residual nodules typically increased in intensity using the hand held device. Frequently, the fluorescence signal from the residual nodule saturated the NIR imaging device. The small residual nodules that could not be detected by the Li-Cor Pearl® Impulse *in vivo* were often visualized *ex vivo*. The fluorescence increased on average 1–2 fold using the NIR imaging device. All tissues were sectioned and underwent H&E staining. All nodules detected by the hand held NIR device were found to have cancer cells (Figure 3b). The signal intensity from peritumoral tissues (ie. muscle, fat, skin) at the margins decreased when imaged *ex vivo* (Figure 3c).

Next, we attempted to determine the smallest residual nodule that could be detected by the imaging system and the Li-Cor Pearl® Impulse. The observers were instructed to measure residual nodules with calipers. There was a poor correlation ($p>0.3$) between size measurements of residual nodules between individuals. Due to the small size of the nodules, this procedure was not technically feasible. All the nodules (n=18) that were under 3 mm in largest diameter (as assessed by the reviewers) were discovered only by the hand held NIR system and not the Li-Cor Pearl® Impulse. Our smallest nodule containing residual disease was less than 2 mm. This nodule had a 5.8 fold increase of signal intensity from background tissue. The Li-Cor Pearl® Impulse was clearly able to detect any nodule that was over 5 mm in largest diameter (n=4).

Together, this data suggests that once a residual nodule is removed from the animal, repeat imaging can be a useful diagnostic test to confirm successful removal. It also permits rapid examination of tumor margins for potentially residual disease, and it provides a valuable resource for surgeons to rapidly determine disease presence in residual tissues without delay in histological confirmation.

Intraoperative detection and removal of residual nodules prevents tumor relapses

In order to determine if imaging could be used to identify residual nodules that could then be removed at surgery (i.e. the “clinical utility”), we repeated the above procedure in 50 mice. Mice were injected with TC1 tumor cells (n=25) and AB12 tumor cells (n=25) into the flank. Once tumors reached $800mm^3$, all of the animals were injected intravenously with ICG and the tumors partially resected 24 hours later. An independent team examined all animals by visual inspection alone and eliminated six animals that had obvious residual nodules. The remaining animals were then randomized to either imaging by the hand held NIR spectroscopic device (n=22) versus no further procedures (n=22). The control animals had their wounds closed, allowed to recover, and were observed. In the other group, we chose an arbitrary 5 fold cutoff (nodule:background signal) for selecting abnormal tissues that were then removed. Twenty of the 22 animals (91%) that were imaged were discovered to have areas of increased IR signal (mean signal 16.9 +/− 3.7 fold difference) and these areas were harvested. One of the remaining animals had a suspicious nodule by NIR imaging (3.8 fold higher fluorescence signal) but did not meet the 5 fold cutoff, therefore, the area was not removed. The other animal did not have any uptake that was discernable despite diligent examination. In addition, we placed this animal in the Li-Cor Pearl® Impulse and did not discover any residual disease, although there was residual fluorescence in the tail vein, which confirmed that mouse had received intravenous ICG. All nodules that were harvested were prepared for histology. All of the animals then had their wounds closed, were allowed to recover, and were observed over time. None of the animals died perioperatively.

All 22 animals that underwent incomplete surgery without imaging developed local flank recurrences within one week. In contrast, only two animals in the group that underwent surgery with image-guided resection developed local recurrences within one week. The 20 animals that underwent successful discovery of residual nodules did not develop recurrences

and were followed for at least 30 days after surgery (Figure 4a). Imaging also appeared to be highly accurate. In every case of resection, pathological examination of the resected material showed the presence of tumor tissue. These data show there was a significant survival advantage to examining the surgical wound for residual disease with the NIR imaging system prior to closing the wound, with only two animals having nodules below the threshold of the hand held device.

ICG fluorescent signal intensity correlates with microvascular density

During our experiments in various cell lines (TC1, AB12, AE17, LLC, 4T1, B16), we noted a significant variation in the fluorescence between cell lines. In our animal experiments above, TC1 tumors consistently expressed the highest fluorescence in recurrent tumors (>35,000 a.u.). AB12 tumors, on the other hand, typically had the lowest fluorescence (~15,000 a.u.). AE17 tumors tended to have fluorescence values that were intermediary of TC1 and AB12. The ratio of background fluorescence to that of the tumor increased in the order of AB12, AE17, and TC1. We thus postulated that the difference in fluorescence is attributable to differing levels of vascularization throughout the tumors which is consistent with the EPR effect (22).

Syngeneic mice underwent injection of TC1, AE17, or AB12 in the right flank. Once tumors reached 800mm^3, they were opened and directly imaged. The tumors were imaged at the center and at four locations 90 degrees apart at the periphery. The average of the peripheral measurements was compared to the average of three readings from the opposite flank. We then harvested the tumors, sectioned them and performed a microvascular density (MVD) assay on TC1, AE17, and AB12 tumors. The assay demonstrated that TC1 tumors have significantly higher vasculature than AB12 tumors (136 vessels/hpf vs. 32, $p < 0.0001$) and AE17 tumors (136 vessels/hpf vs. 62, $p < 0.0001$) thus providing one potential explanation for the difference in fluorescence between tumors (Figure 4b).

Canine model of soft tissue sarcoma confirms NIR imaging of tumor margins

Three canines with soft tissue sarcomas were resected between December 2011 and April 2012 by standard veterinary practice. During the operation, all three tumors could be easily palpated and tumor margins were evident by visualization and palpation by the veterinary surgeon (Figure 5a). *In vivo* imaging was able to detect all tumor margins without difficulty (Figure 5a). All tumors had 12 to 15 fold increased fluorescence compared to surrounding tissue. No residual tumor deposits were discovered in the surgical bed after tumor resection. After removing the soft tissue sarcomas, the tumors were analyzed for tumor margins using the hand held NIR imaging device (Figure 5b). All resection margins were negative for any evidence of cancer deposits. All tumors were ultimately discovered to have negative margins by histopathology. No local recurrences have been detected to date in these three canine patients (follow up 45–110 days).

Discussion

Over the last two centuries, surgeons have depended on two tools in the operating room to detect disease – their eyes to look for suspicious masses and their hands to feel for abnormal tissue (23). Surgeons make subjective decisions based on experience of anatomical tissue planes and tumor spread in deciding where to excise tumors to obtain disease-free margins. However, this is historically inaccurate, especially in complex fields including those with prior radiation, infection or trauma. For example, at University of Miami, one experienced urologist performed 100 consecutive radical prostatectomies and recorded intra-operatively if he suspected the tumor margins were positive or negative based on visual clues and palpation (24). Despite his intra-operative decision that the surgical margins were negative

in all 100 patients, the true pathological margins were positive in 39% of cases. The intra-operative assessment of the margin status had a high false-negative rate and a sensitivity of only 7%. The sensitivity of the intra-operative assessment of tumor location was 73%, and the positive predictive value was 65%. Our results confirm that visual inspection and manual palpation alone are insufficient for discovering residual tumor nodules (Figures 1, 2 and 4a). This work proposes using near infrared imaging techniques, in real-time, during surgery for accurate discovery of residual disease in the surgical wound. This work demonstrates this approach using an FDA approved fluorophore and a novel imaging device that is compact and hand-held.

Several techniques have been developed to assist surgeons improve upon intra-operative decision-making. For example, rapid pathological frozen section can be used to verify the entire tumor has been removed. The pathologist will microscopically study a few limited locations on the specimen to determine if residual tumor cells remain in the patient before the surgeon ends the operation. Although frozen section does improve assessment of surgical margins, it also has limited sensitivity and practicality (25). Routine frozen section analysis is time-consuming and can lead to inadequate assessment of tumor margins in large specimens and loss of diagnostic material in small specimens (26). Time-intensive techniques, such as frozen section analysis, also have the disadvantage of prolonging the surgical procedure and thereby the time the patient remains anesthetized. In order to improve accuracy from 90% to 99% for detecting cancer requires the pathologist to triple the number of blocks to be examined (27).

Near infrared fluorophores are probes that emit at 700–850 nm and have significant advantages for imaging due to minimal interfering absorption and fluorescence from biological samples, inexpensive laser diode excitation, reduced scattering, and enhanced tissue penetration depth (28). To date, only one NIR probe, indocyanine green (ICG), has been approved by the Food and Drug Administration. ICG, is a water-soluble, anionic, amphiphilic tricarbocyanine probe with a hydrodynamic diameter of 1.2 nm, and excitation and emission wavelengths in serum at 778 and 830, respectively. ICG has been in clinical use since the 1950’s for ophthalmic angiography, determining cardiac output and hepatic function measurements. However, it has only recently shown real practicability and feasibility in the field of surgical oncology (9).

Near infrared fluorophores such as ICG can be delivered to tumors via a passive targeting mechanism. Nanometer-sized particles accumulate preferentially at tumor sites through an enhanced permeability and retention (EPR) effect (10, 11). In order for tumor cells to grow, they stimulate a complex process of tumor angiogenesis. Tumor cell deposits as small as 200 nm depend on hypervascularization and extensive production of vascular permeability factors to deliver oxygen and nutrients. These vessels are characterized by defective endothelial cells that have wide fenestrations, lack a smooth muscle layer, and have wide lumens. In addition, these tumor deposits lack efficient vascular and lymphatic drainage, which leads to abnormal molecular and fluid transport dynamics (11). As a consequence, small molecules such as ICG can readily leak into the cancer tissues. Once in this acidic tumor microenvironment, ICG will preferentially bind albumin and other tissue proteins that cause it to accumulate over time. In our study, we found a direct correlation with highly vascular murine tumors and ICG fluorescence (Figure 4b). Human cancers that have been well-formed may not have leaky capillaries on the interior, however, we postulate the outer border, ie. the surgical margin, may be expected to have a stronger EPR effect.

Due to the retention of ICG in tumor tissue, NIR imaging can locate residual nodules after surgery (Figure 2a). Although there is substantial background fluorescence in the surrounding tissue, ICG uptake in tumors is over 15 fold higher (Figure 2b, Figure 5).

Attempts to diminish the dose of ICG decreased the background fluorescence, but also reduced the fold difference between the tumor and normal tissues (data not shown). Increasing the dose of ICG did not significantly improve imaging quality, thus our group chose to use 7.5 mg/kg. There was no concern of toxicity with ICG in this dose range as the LD_{50} for this agent is in the order of 80–100 mg/kg. Synchronous labeling of murine cancer cells with green fluorescent protein as demonstrated in other models for image guided surgery (8) was also successful in our study to validate sensitivity for residual tumor tissue in our model (Figure 2c).

NIR imaging systems such as the Li-Cor Pearl® Impulse are useful for animal studies, however, our previously described hand held device is more practical for human application (17). In this trial, we found a hand held device to be significantly more sensitive than the Li-Cor Pearl® Impulse. This is partially due to the ability to hold the device in close proximity to the tissue that is being examined.

These studies raised several concerns that may limit this technology's full potential to locate tumor nodules. First, we acknowledge a small animal model of surgery is less than ideal to assess positive margins, particularly in the flank. However, we have created a reproducible model that can be performed with consistent residual disease that is not palpable or visually obvious. Our preliminary studies with a spontaneous canine tumor model are promising. Second, the ICG is excreted via the biliary system, thus any tumors close to the liver cannot be assessed due to the high level of background. Third, we do not feel at this point we have sufficient data to conclude 7.5 mg/kg is the best dose for visualizing residual disease. We have had similar success with smaller doses as well as utilizing multiple doses, which will be addressed in future studies. In addition, it is not clear if the size of the original tumor could correlate with the fluorescence of tumor margins. Unfortunately, this is one significant limitation of this model and will likely need to be addressed in larger animal models or humans. Fourth, we emphasize that ICG is limited in clinical scope due to its non-specific nature. It diffuses into any regions of vascular permeability, hence, both inflammatory and neoplastic areas are likely to be highlighted. The surgeon will be required to use alternative clues to judge whether the area should be removed. Finally, depth of penetration in imaging ICG will be a limiting factor for more complex resections where the lesion of concern is behind other tissues. However, this study was performed using ICG because it is currently the only FDA approved contrast agent. Alternative particles do exist which permit deeper tissue penetration, but they would require higher excitation energy sources. For purposes of margins, however, this approach is feasible and efficacious as demonstrated in this work.

This approach towards imaging intraoperatively had other advantages that should be acknowledged. In addition to assessing tumor margins, it is accurate for "back table" assessment after resection (Figure 3c). Although frozen section will remain the gold standard, this approach has a superb advantage in rapidly examining residual tissue before delaying the case for pathological analysis. In conclusion, this work adds a novel approach to rapidly assessing the surgical wound for residual disease with low toxicity, high sensitivity and may add to the surgeon's armamentarium in judging completeness of resection.

Acknowledgments

The authors would like to acknowledge Dr. Steven M. Albelda for his valuable input in experimental design and manuscript review.

Grant Support

This work was supported by the National Institutes of Health Grand Opportunities Grant RC2CA148265 (M.W., S.N., S.S.) & Society of Surgical Oncology Clinical Scholar Award (S.S.) & American Kennel Club Acorn Grant (D.H., S.S.).

References

1. Jemal A, Siegel R, Xu J, Ward E. Cancer statistics, 2010. CA Cancer J Clin. 2010; 60:277–300. [PubMed: 20610543]
2. Aliperti LA, Predina JD, Vachani A, Singhal S. Local and systemic recurrence is the Achilles heel of cancer surgery. Ann Surg Oncol. 2011; 18:603–607. [PubMed: 21161729]
3. Menes TS, Tartter PI, Bleiweiss I, Godbold JH, Estabrook A, Smith SR. The consequence of multiple re-excisions to obtain clear lumpectomy margins in breast cancer patients. Ann Surg Oncol. 2005; 12:881–885. [PubMed: 16195834]
4. Carter D. Margins of "lumpectomy" for breast cancer. Hum Pathol. 1986; 17:330–332. [PubMed: 3957334]
5. Abraham SC, Fox K, Fraker D, Solin L, Reynolds C. Sampling of grossly benign breast reexcisions: a multidisciplinary approach to assessing adequacy. Am J Surg Pathol. 1999; 23:316–322. [PubMed: 10078923]
6. Schaafsma BE, Mieog JS, Hutteman M, van der Vorst JR, Kuppen PJ, Lowik CW, et al. The clinical use of indocyanine green as a near-infrared fluorescent contrast agent for image-guided oncologic surgery. J Surg Oncol. 2011
7. De Grand AM, Lomnes SJ, Lee DS, Pietrzykowski M, Ohnishi S, Morgan TG, et al. Tissue-like phantoms for near-infrared fluorescence imaging system assessment and the training of surgeons. J Biomed Opt. 2006; 11 014007.
8. Kishimoto H, Zhao M, Hayashi K, Urata Y, Tanaka N, Fujiwara T, et al. In vivo internal tumor illumination by telomerase-dependent adenoviral GFP for precise surgical navigation. Proc Natl Acad Sci U S A. 2009; 106:14514–14517. [PubMed: 19706537]
9. Polom K, Murawa D, Rho YS, Nowaczyk P, Hunerbein M, Murawa P. Current trends and emerging future of indocyanine green usage in surgery and oncology: A Literature Review. Cancer. 2011
10. Singhal S, Nie S, Wang MD. Nanotechnology applications in surgical oncology. Annu Rev Med. 2010; 61:359–373. [PubMed: 20059343]
11. Greish K. Enhanced permeability and retention of macromolecular drugs in solid tumors: a royal gate for targeted anticancer nanomedicines. J Drug Target. 2007; 15:457–464. [PubMed: 17671892]
12. Davis MR, Manning LS, Whitaker D, Garlepp MJ, Robinson BW. Establishment of a murine model of malignant mesothelioma. Int J Cancer. 1992; 52:881–886. [PubMed: 1459729]
13. Predina JD, Judy B, Aliperti LA, Fridlender ZG, Blouin A, Kapoor V, et al. Neoadjuvant in situ gene-mediated cytotoxic immunotherapy improves postoperative outcomes in novel syngeneic esophageal carcinoma models. Cancer Gene Ther. 2011; 18:871–883. [PubMed: 21869822]
14. Predina JD, Judy B, Kapoor V, Blouin A, Aliperti LA, Levine D, et al. Characterization of surgical models of postoperative tumor recurrence for preclinical adjuvant therapy assessment. Am J Transl Res. 2012; 4:206–218. [PubMed: 22611473]
15. Tiscornia G, Singer O, Verma IM. Production and purification of lentiviral vectors. Nat Protoc. 2006; 1:241–245. [PubMed: 17406239]
16. Predina JD, Judy B, Fridlender ZG, Aliperti LA, Madajewski B, Kapoor V, et al. A positive-margin resection model recreates the postsurgical tumor microenvironment and is a reliable model for adjuvant therapy evaluation. Cancer Biol Ther. 2012; 13
17. Mohs AM, Mancini MC, Singhal S, Provenzale JM, Leyland-Jones B, Wang MD, et al. Hand-held Spectroscopic Device for In Vivo and Intraoperative Tumor Detection: Contrast Enhancement, Detection Sensitivity, and Tissue Penetration. Anal Chem. 2010
18. Jensen MM, Jorgensen JT, Binderup T, Kjaer A. Tumor volume in subcutaneous mouse xenografts measured by microCT is more accurate and reproducible than determined by 18F-FDG-microPET or external caliper. BMC Med Imaging. 2008; 8:16. [PubMed: 18925932]

19. Baldwin HS, Shen HM, Yan HC, DeLisser HM, Chung A, Mickanin C, et al. Platelet endothelial cell adhesion molecule-1 (PECAM-1/CD31): alternatively spliced, functionally distinct isoforms expressed during mammalian cardiovascular development. Development. 1994; 120:2539–2553. [PubMed: 7956830]

20. Judy BF, Aliperti LA, Predina JD, Levine D, Kapoor V, Thorpe PE, et al. Vascular endothelial-targeted therapy combined with cytotoxic chemotherapy induces inflammatory intratumoral infiltrates and inhibits tumor relapses after surgery. Neoplasia. 2012; 14:352–359. [PubMed: 22577350]

21. Predina JD, Kapoor V, Judy BF, Cheng G, Fridlender ZG, Albelda SM, et al. Cytoreduction surgery reduces systemic myeloid suppressor cell populations and restores intratumoral immunotherapy effectiveness. J Hematol Oncol. 2012; 5:34. [PubMed: 22742411]

22. Greish K. Enhanced permeability and retention (EPR) effect for anticancer nanomedicine drug targeting. Methods Mol Biol. 2010; 624:25–37. [PubMed: 20217587]

23. Ellis MC, Hessman CJ, Weerasinghe R, Schipper PH, Vetto JT. Comparison of pulmonary nodule detection rates between preoperative CT imaging and intraoperative lung palpation. Am J Surg. 2011; 201:619–622. [PubMed: 21545910]

24. Vaidya A, Hawke C, Tiguert R, Civantos F, Soloway M. Intraoperative T staging in radical retropubic prostatectomy: is it reliable? Urology. 2001; 57:949–954. [PubMed: 11337301]

25. Klimberg VS, Harms S, Korourian S. Assessing margin status. Surg Oncol. 1999; 8:77–84. [PubMed: 10732959]

26. Ferreiro JA, Gisvold JJ, Bostwick DG. Accuracy of frozen-section diagnosis of mammographically directed breast biopsies. Results of 1,490 consecutive cases. Am J Surg Pathol. 1995; 19:1267–1271. [PubMed: 7573688]

27. de Mascarel I, Trojani M, Bonichon F, Coindre JM. Histological examination of 2859 breast biopsies. Analysis of adequate sampling. Pathol Annu. 1993; 28(Pt 1):1–13. [PubMed: 8416134]

28. Gioux S, Choi HS, Frangioni JV. Image-guided surgery using invisible near-infrared light: fundamentals of clinical translation. Mol Imaging. 2010; 9:237–255. [PubMed: 20868625]

Statement of Translational Relevance

In the United States, over 700,000 people undergo cancer surgery each year for curative intent. Up to 40% of those patients develop local recurrences within 5 years of their initial operation, likely due to missed cancer deposits. Our group has developed a novel approach to image for residual cancer during surgery to confirm disease clearance. This approach uses a safe, non-toxic, non-radioactive strategy using indocyanine green, an FDA approved near-infrared fluorophore. Multiple cancer type mouse models were utilized to demonstrate its utility. This data is currently being used to move forward with a Phase I/II clinical trial for patients with breast cancer and lung cancer. This unique tactic of intraoperative imaging with near-infrared techniques will likely impact all fields of Surgical Oncology within the next decade.

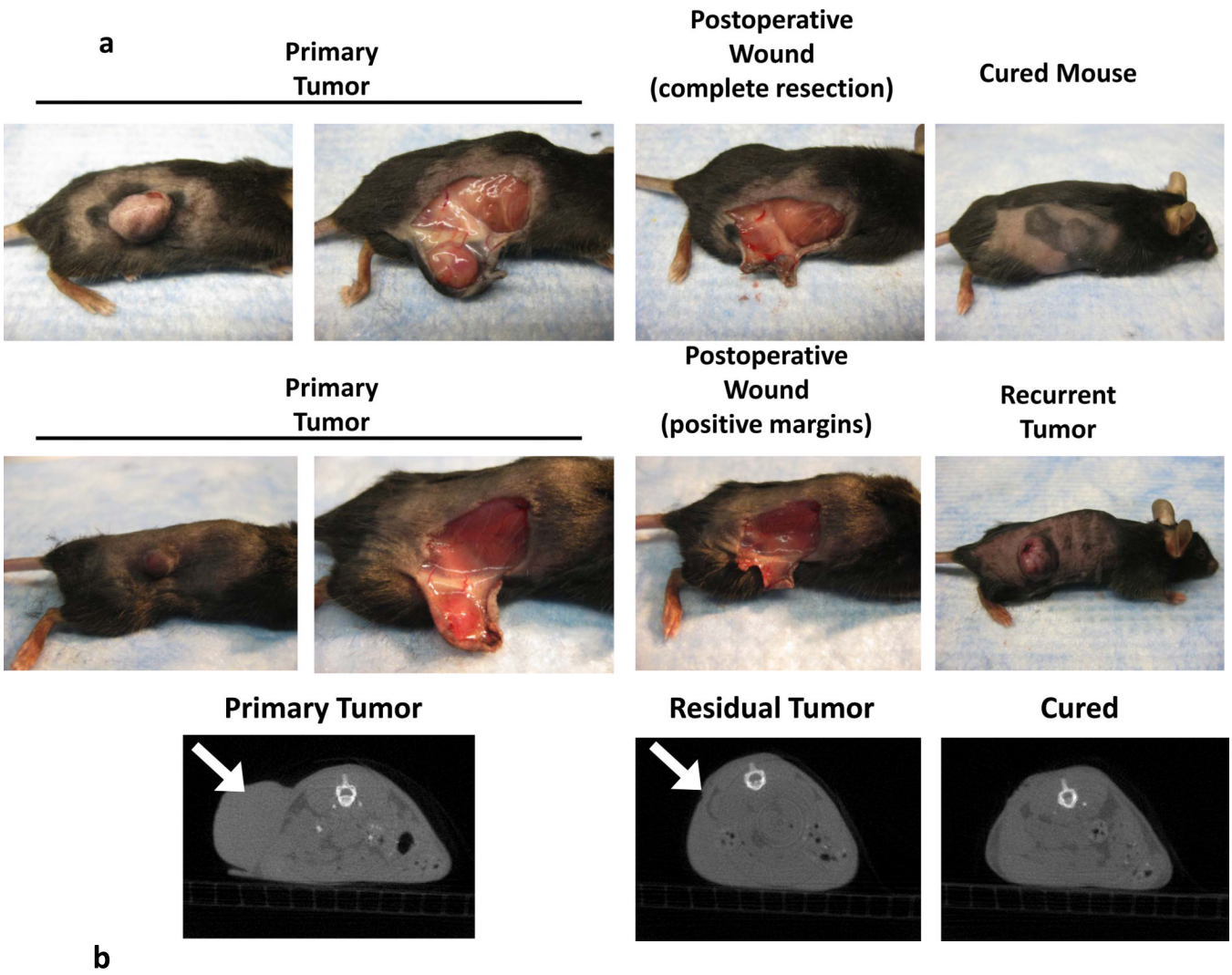

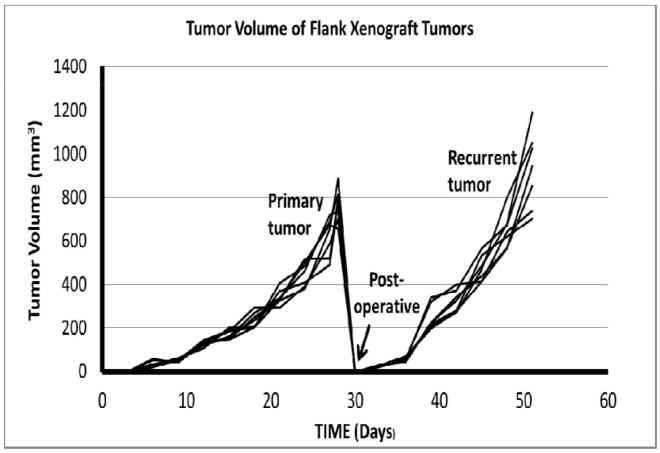

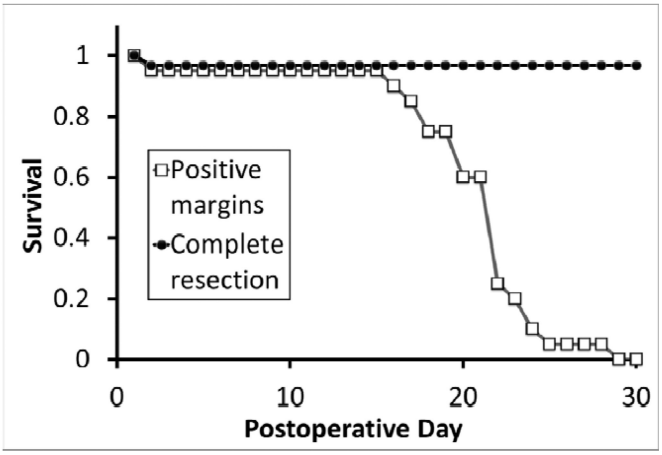

Figure 1.

A surgical model for local recurrence of disease following surgery. Syngeneic immunocompetent mice were injected with 1.5e6 TC1 tumor cells into the right flank (not over the liver) and developed large tumors (>800 mm^3). When the tumors measured 800mm^3, they were either partially resected with positive margins or completely removed. In the partial resection group, the surgeon used a #15 scalpel to sharply divide the tumor and leave the smallest possible residual nodule (<5%) that was technically feasible (ranged 2 to 4 mm in diameter). This tumor deposit was typically left attached to either the skin or underlying muscle. (A) A representative animal from each group is shown. Two independent observers first visually inspected the wound, and then palpated the wound in order to determine which animals had residual disease versus curative surgery. Animals (n=20) without obvious tumor to independent observers underwent microCT scans to determine if residual disease could be radiographically located. White arrows designate flank tumors. (B) Following surgical intervention, all animals with (i) positive margins and (ii) total resections were monitored for recurrence of their flank tumors. Tumor volume vs time and Kaplan Meier survival curves for a typical flank TC1 (n=20) experiment are depicted.

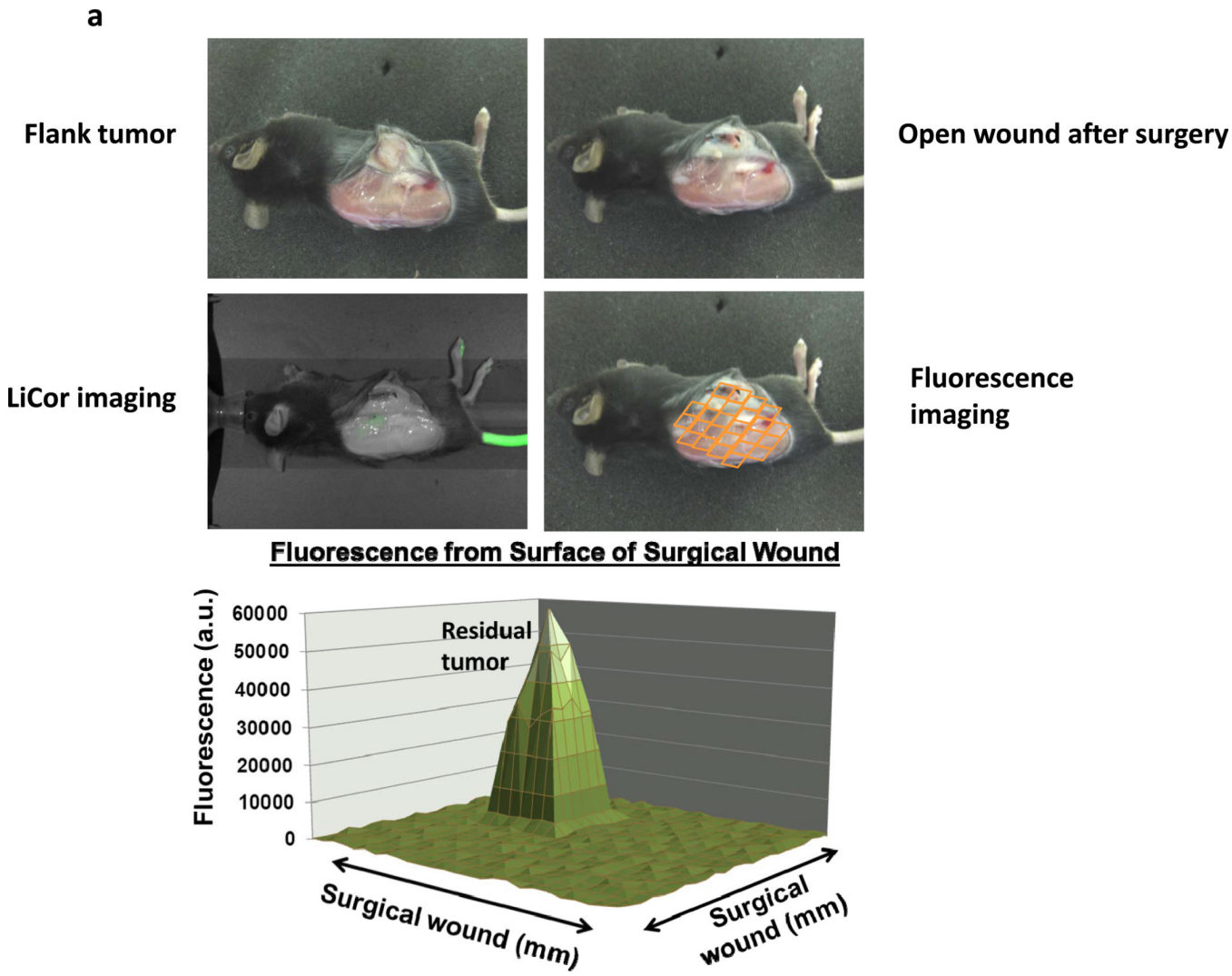

b

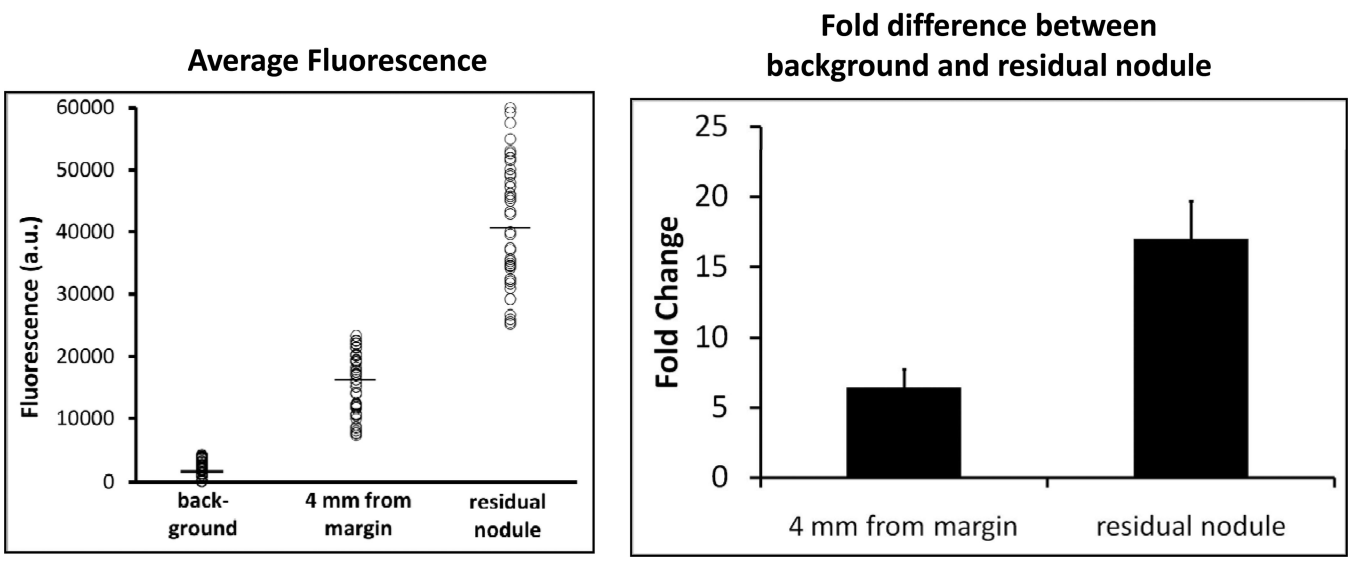

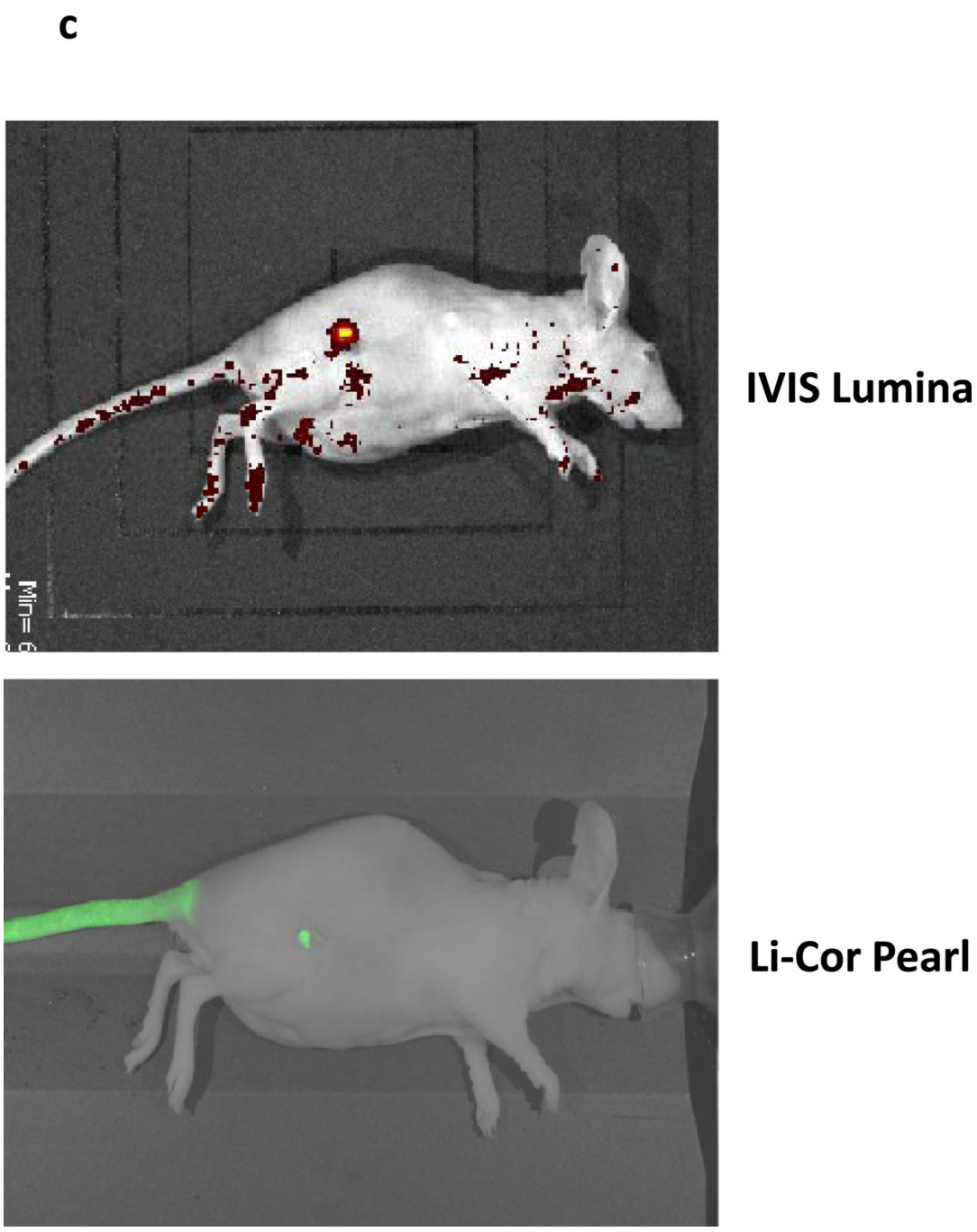

Figure 2.

Residual disease in the surgical bed fluoresces after incomplete resection. C57bL/6 mice were injected with 1.5e6 TC1 cells into the right flank. Once tumors reached 800mm^3, animals were intravenously injected with 7.5 mg/kg ICG intravenously. Twenty-four hours later, the surgeon sharply removed 95% of the tumor with minimal residual disease. Two independent observers were then designated to locate suspicious margins. If residual disease was detected, the animal was eliminated from the study. The remaining animals had their surgical bed imaged by the Li-Cor Pearl® Impulse. The surgical field was then arbitrarily assigned a virtual grid and three readings using the NIR hand held machine were recorded and averaged in each sector. The mean background value was calculated from this data. If a

region of high fluorescence was detected, serial readings were performed circumferentially at 2 mm intervals surrounding the suspicious location. (A) A representative C57bl/6 mouse with a flank TC1 is depicted. After surgical resection, the residual nodule could not be visualized by two independent observers or with assistance from the Li-Cor Pearl® Impulse. The hand held device rapidly detected the lesion and a typical map of the surgical wound is presented. (B) The mean fluorescence from the residual nodules (n=54) and the peritumoral tissue 4 mm from the margin is shown in the bubble graph. The fold difference between the background signal, 4mm margin and actual residual nodule are represented in the bar graph. (C) Duplicate experiments were performed in mice bearing AE17-GFP tumors in order to evaluate if ICG expression was occurring in residual tumors versus leaking into surrounding tissues following the surgery.

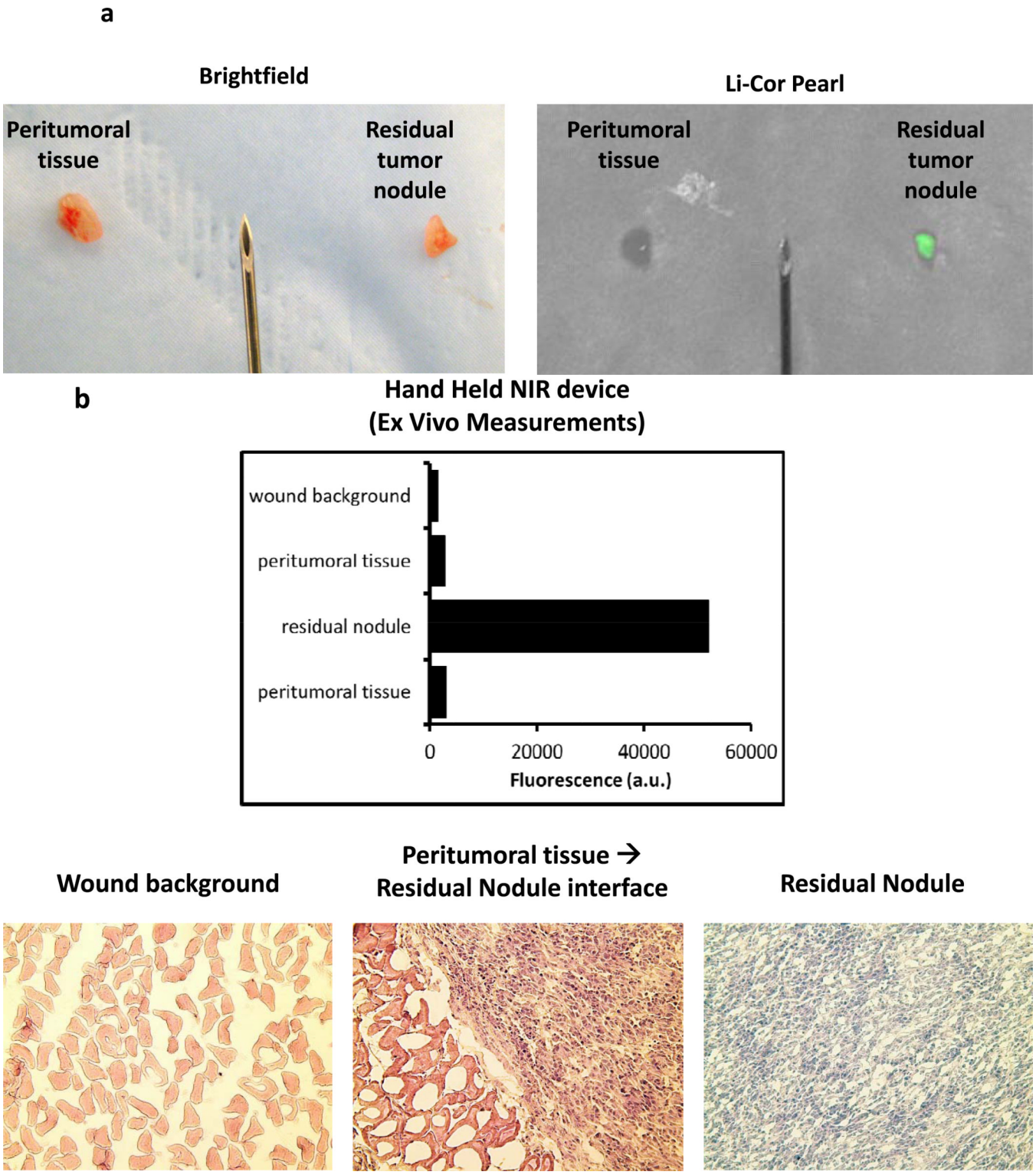

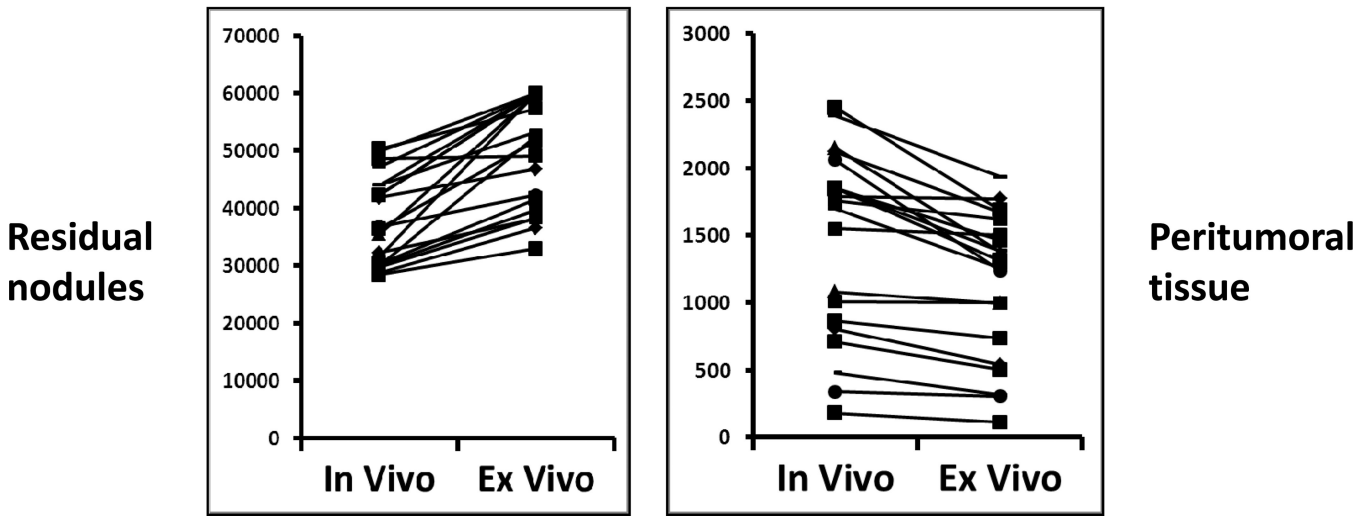

Figure 3.

Residual tumor deposits have elevated fluorescent signals *ex vivo*. Following intraoperative imaging, residual nodules that were detected by the NIR imaging system were harvested. (A) A representative tumor nodule (right) is detected adjacent to a 25 gauge hypodermic needle (outer diameter 0.51 mm). Additional peritumoral adipose tissue was harvested for comparison (left). Li-Cor Pearl® Impulse imaging and NIR imaging from the hand held device was performed on all specimens once they were removed from the experimental animals. (B) *Ex vivo* fluorescence of the background tissue, peritumoral tissue and the residual nodule. H&E staining was used to confirm residual cancer cells in all experiments. (C) *In vivo* fluorescence of murine cancerous and non-cancerous tissues was compared to the fluorescence *ex vivo* after surgery.

a

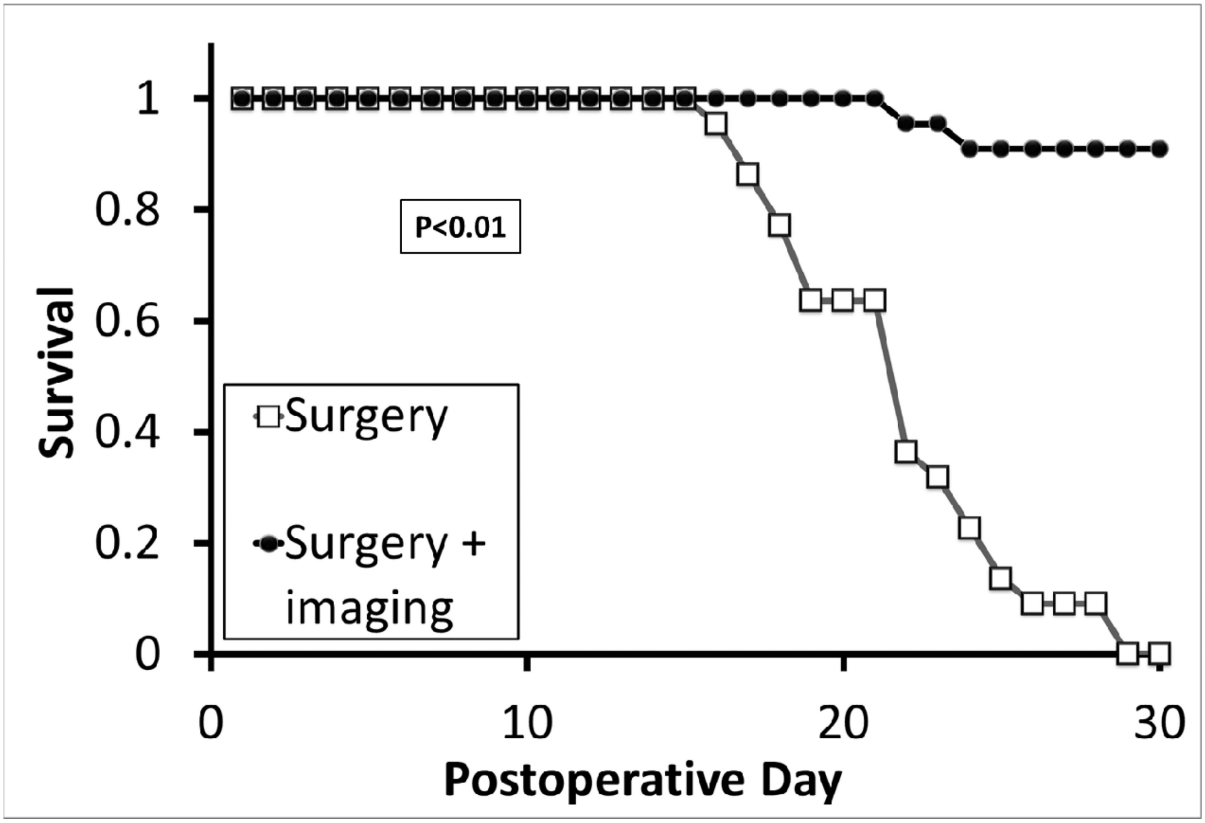

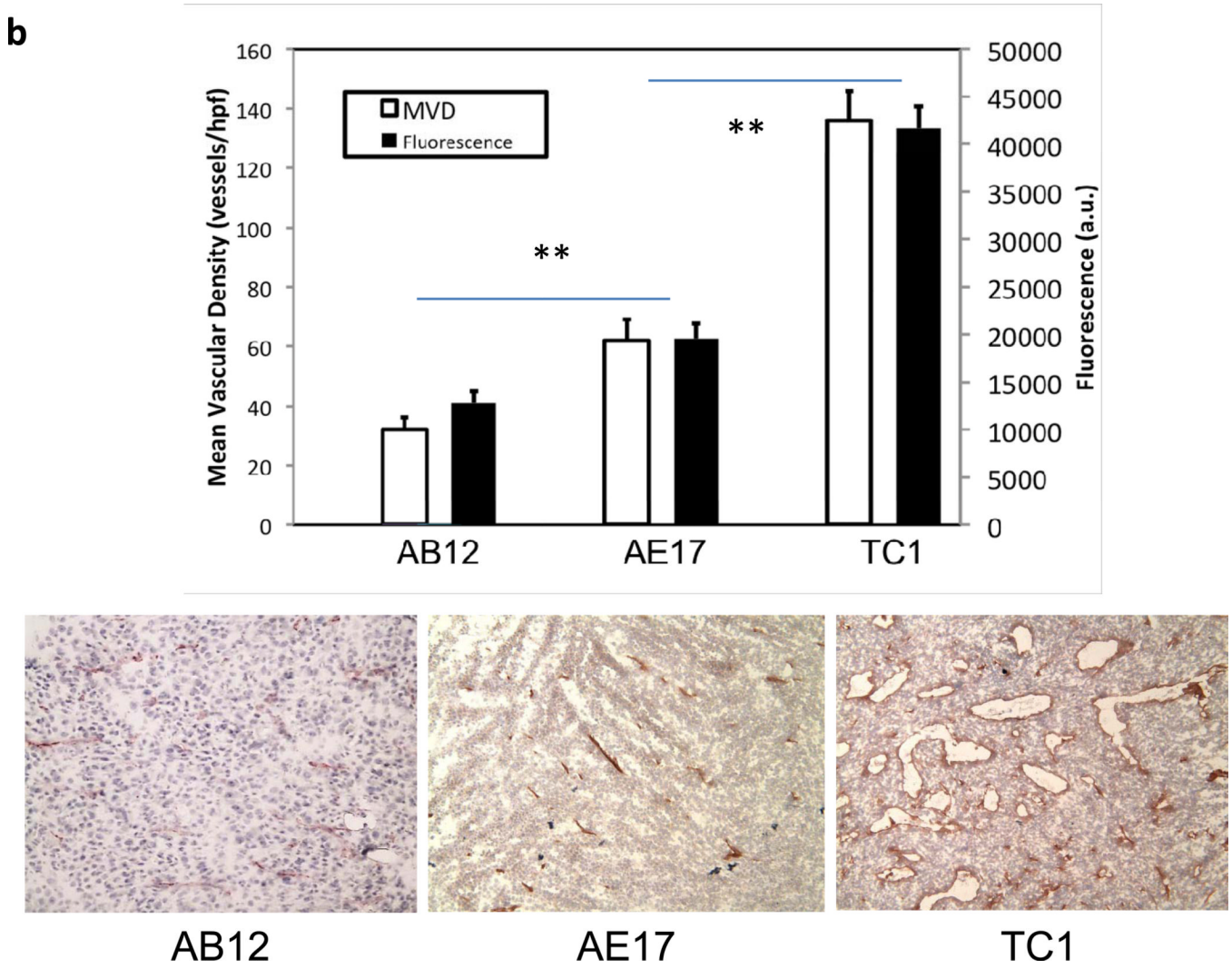

Figure 4.

(A) Intraoperative detection of residual nodules after surgical resection prevents tumor relapses. In two separate experiments, syngeneic mice were injected with TC1 or AB12 tumor cells into the flank. Once tumors reached 800mm^3, the animals were injected with ICG via tail vein and then partially resected 24 hours later. Again, two independent observers examined all animals and eliminated any mice with obvious residual disease. These animals were then chosen to undergo imaging by the hand held NIR spectroscopic device or to have their wounds closed without any further procedures. If the hand held device detected a signal that was 5 times higher than the background for the surgical bed, the abnormal tissue was removed. A Kaplan Meier survival curve for the flank TC1 (n=25) experiment is depicted. (B) Animals were injected with TC1 or AB12 cell lines and tumors were allowed to grow to 800mm^3. The tumors were imaged by the hand held imaging device in 5 locations and averaged. Tumors were harvested, sectioned and underwent a microvascular density assay using monoclonal CD31 staining. ** indicates a p value of < 0.01.

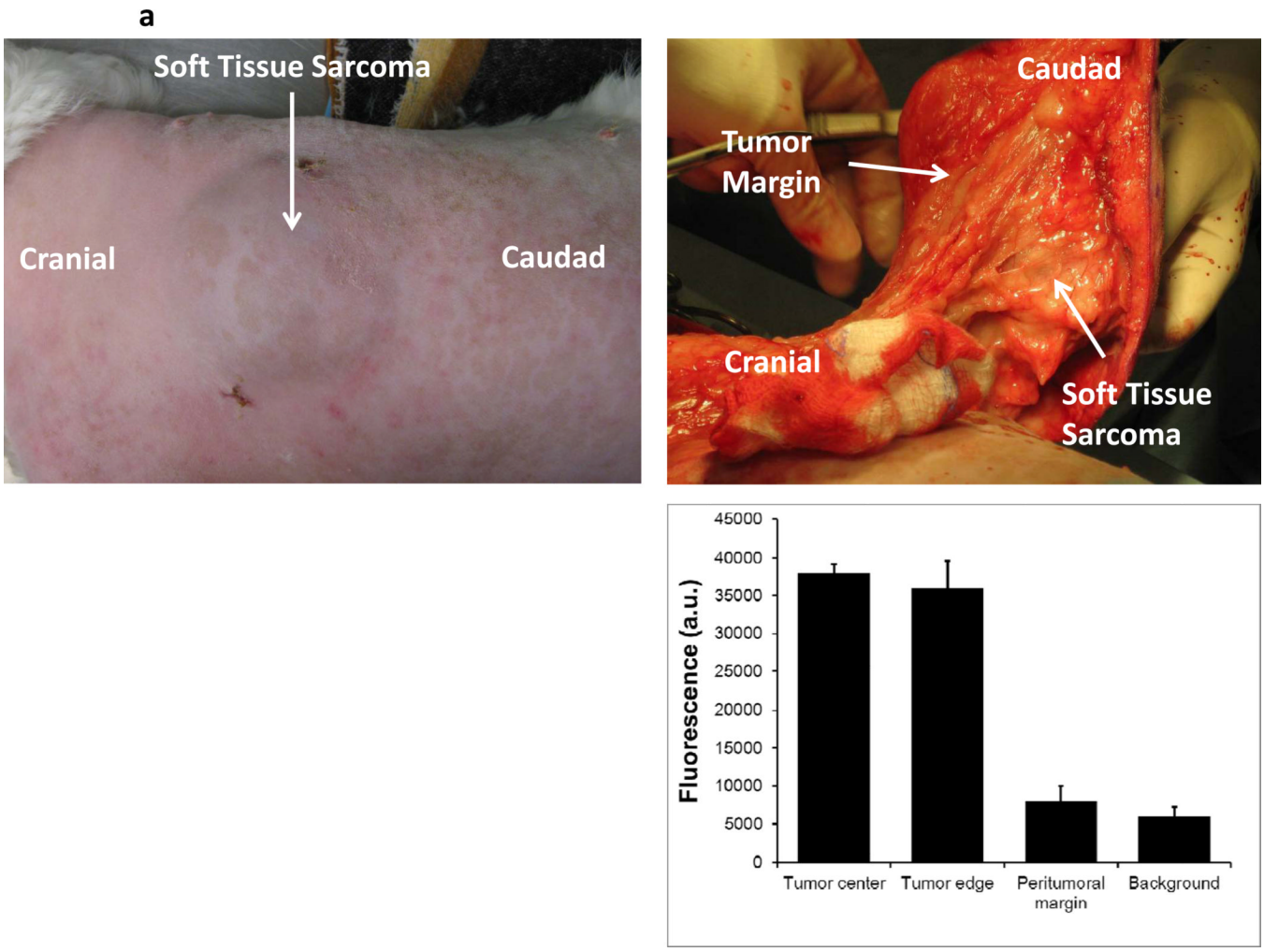

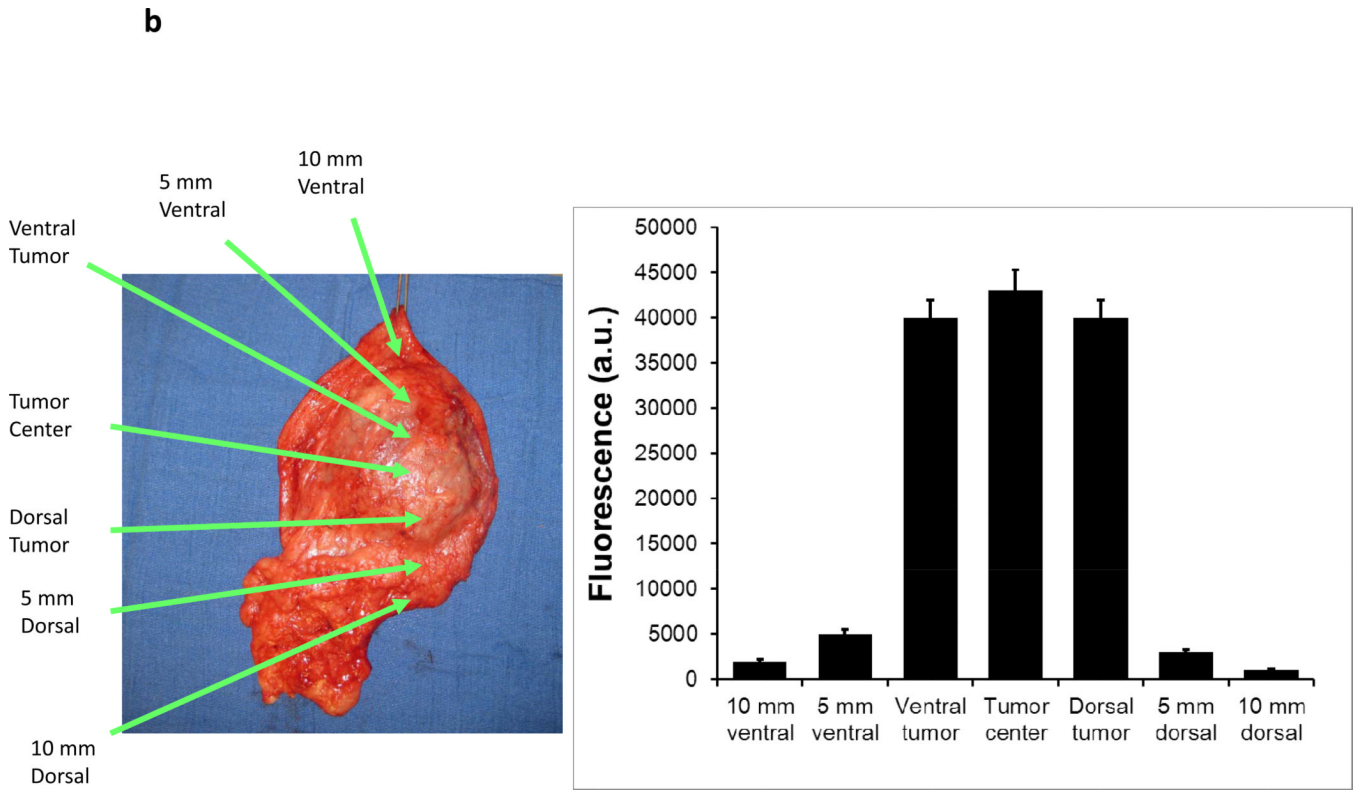

Figure 5.

A canine with a spontaneous abdominal wall sarcoma underwent image guided surgery. After ICG injection, (A) a canine abdominal was opened to reveal a well demarcated soft tissue sarcoma. The primary tumor was imaged in 8 radial directions from the center of the tumor and fluorescence averaged. The tumor bed was imaged prior to wound closure. (B) After resection, *ex vivo* fluorescence measurements were again performed.